

## Highlights

### **A Decision-Making Model for Retired Li-ion Batteries**

Jihan Zhuang, Amadeus Bach, Bruis H. C. van Vlijmen, Stefan J. Reichelstein, William Chueh, Simona Onori, Sally M. Benson

- A systematic framework is built for decision-making model of second life batteries.
- Data-driven models and Monte Carlo method are applied to simulate the module-level aging performance of second life batteries.
- An economic model is integrated with aging model to evaluate the price of retired batteries under different second life applications.
- The decision between recycling and reusing is made upon various second life use cases.

# A Decision-Making Model for Retired Li-ion Batteries

Jihan Zhuang<sup>a,c,\*</sup>, Amadeus Bach<sup>b</sup>, Bruis H. C. van Vlijmen<sup>a,c</sup>, Stefan J. Reichelstein<sup>b,d</sup>, William Chueh<sup>a</sup>, Simona Onori<sup>e,\*\*</sup> and Sally M. Benson<sup>e,\*\*</sup>

<sup>a</sup>Materials Science and Engineering Department, Stanford University, 450 Serra Mall, Stanford, 94305, California, United States

<sup>b</sup>Mannheim Institute for Sustainable Energy Studies, University of Mannheim, Mannheim, Germany

<sup>c</sup>SLAC National Accelerator Laboratory, Menlo Park, 94025, California, United States

<sup>d</sup>Graduate School of Business, Stanford University, Stanford, 94305, California, United States

<sup>e</sup>Energy Science and Engineering Department, Stanford University, 450 Serra Mall, Stanford, 94305, California, United States

## ARTICLE INFO

### Keywords:

Second life battery

Decision-making model

Data-driven model

Module-level aging model

## ABSTRACT

The growth of electric vehicles (EVs) has raised concerns about the disposition of their batteries once they reach their end of life. Currently, recycling is regarded as the potential solution for retired Li-ion batteries (LIBs). However, these LIBs still retain around 80% of their original capacity, which can be repurposed for other energy storage system (ESS) applications in their "second life" before recycling. Yet, there is no guidance for deciding whether to reuse or recycle them. Here, we propose developing a decision-making model that evaluates retired batteries from both technical and economic perspectives. We develop data-driven models and combine them with an equivalent circuit model (ECM) to build module-level aging models. Simulations show that limiting the State of Charge (SOC) operating range and charge current in second life applications can extend the lifetime of LIBs. Upon when and how to use the battery in second life, the simulated lifetime is between 1-6 years. From an economic perspective, we find that the most profitable application is frequency regulation, which has a value of 273.4\$  $kWh^{-1}$ . We present a comprehensive comparison of different end-of-life strategies to demonstrate the most economically way to handle a retired battery.

## 1. Introduction

The issue of global energy sustainability is one of the most significant challenges facing humanity today. Transportation alone accounts for 28% of worldwide energy consumption, highlighting the critical need for clean and efficient transportation solutions (a). Electric vehicles (EVs) represent a promising solution to address this issue, but managing retired EV batteries remains a challenge. By 2030, the widespread adoption of EVs is expected to generate a surplus of 100-200 gigawatt-hours of batteries that no longer meet the necessary specifications for continued use in EVs (Zhu, Mathews, Ren, Li, Cogswell, Xing, Sedlatschek, Kantareddy, Yi, Gao, Xia, Zhou, Wierzbicki and Bazant (2021)). While recycling these batteries and extracting raw materials is the most established approach (Chen, Ma, Chen, Arsenault, Karlson, Simon and Wang (2019)), the current recycling capacity is limited. Companies like Li-Cycle aims to recycle only 35 kilo-tonnes of batteries by 2030, far below the projected 80 kilo-tonnes of retired lithium-ion batteries in 2030 (JEAN KUMAGAI). In addition, the LIBs in Tesla cars exhibit only a 10% degradation even after 200,000 miles (Justin Westbrook), indicating the batteries remain healthy when other components may start to deteriorate after 10 years of service. Consequently, directly recycling the batteries after the EV service may not always be the optimal choice in this scenario. To find an alternative solution, researchers are exploring the potential to reuse retired batteries in Energy Storage Systems (ESS) as their second life applications (Zhu et al. (2021)). This approach can reduce battery costs, extend the lifespan of these batteries, and thus provide a sustainable solution to the circular economy. Furthermore, second life batteries (SLBs) could serve as a cheaper source of electricity, aiding developing countries in improving their quality of life and electrifying their industries in a more sustainable way (Kebir, Leonard, Downey, Jones, Rabie, Bhagavathy and Hirmer), thereby promoting equity and helping them achieve net-carbon-emission goals.

\*Corresponding author

\*\*Principal corresponding author

✉ jihan123@stanford.edu (J. Zhuang)

ORCID(s): 0009-0003-9140-1028 (J. Zhuang)

In recent years, research articles and industrial reports have explored the economical feasibility of SLBs for ESSs. Baumann et al. Baumann, Rohr and Lienkamp and Seger et al. Seger, Thivel and Riu have attempted to address the technical challenges of SLBs, including lifetime estimation using battery aging models. Other studies have focused on the economic viability of SLBs, analyzing repurposing costs and price estimation Mathews, Xu, He, Barreto, Buonassisi and Peters; Börner, Friege, Späth, Spütz, Heimes, Sauer and Li; Sun, Chipperfield, Kiaee and Wills (2018). Furthermore, commercial companies such as Toyota noa (b) and Mercedes Duarte have launched demonstration projects to assess the economical feasibility of SLB. Nonetheless, the recycling versus reusing debate is still ongoing, given the lack of experimental data and model proofing. No comprehensive decision-making model exists for the end-of-life strategy for different retired Li-ion batteries, considering both technical and economic perspectives. As discussed in a recent review paper, the authors pointed out that the most common and urgent demand is to have a comprehensive battery evaluation tool and a battery passport Zhu et al. (2021), which refers to a battery dataset containing the battery chemistry and usage profile. To address this gap, our paper proposes a novel decision-making model that can hopefully solve the ongoing debate between recycling and reusing of SLBs. Our model also calls for the implementation of battery passport in United States.

### 1.1. The aging model for second life battery

Current models for predicting Li-ion battery degradation are mostly focused on individual battery cells and their first life Xiong, Li and Tian Lucu, Martinez-Laserna, Gandiaga and Camblong. These models can be categorized into physics-based models Prada, Di Domenico, Creff, Bernard, Sauvart-Moynot and Huet, Pinson and Bazant, Weaver, Allam and Onori (2020), Arunachalam and Onori (2019), empirical models (including semi-empirical models) Chu, Allam, Cordoba Arenas, Rizzoni and Onori (2020), Petit, Prada and Sauvart-Moynot (2016), Rechkemmer, Zang, Zhang and Sawodny (2019), and data-based models Hu, Che, Lin and Onori (2021), Severson, Attia, Jin, Perkins, Jiang, Yang, Chen, Aykol, Herring, Fraggadakis, Bazant, Harris, Chueh and Braatz, Attia, Grover, Jin, Severson, Markov, Liao, Chen, Cheong, Perkins, Yang, Herring, Aykol, Harris, Braatz, Ermon and Chueh. In recent years, machine learning (ML) models have gained significant attention in academia and industry due to high prediction accuracy with low computational and labor costs Ng, Zhao, Yan, Conduit and Seh. However, with the inhomogeneity of cells in a module, the uncertainty related to aging increases significantly as the battery degrades Tanim, Shirk, Bewley, Dufek and Liaw, Johnen, Pitzten, Kamps, Kateri, Dechent and Sauer. In addressing the challenge of uncertainty in degradation, probabilistic ML methods are widely applied Jones, Stimming and Lee, since most ML models are deterministic. Gaussian process regression (GPR) is one of the stochastic methods that incorporates uncertainties into the prediction process Richardson, Osborne and Howey (2017). More specifically, GPR calculates the probability distribution over all admissible functions that fit the data, resulting in outputs that are not single values but rather a range of possible values with uncertainties. This aligns perfectly with the nonlinear and complex nature of battery degradation. In the literature, Yang et al. Yang, Zhang, Pan, Wang and Chen applied the GPR technique to estimate the battery SOH. Another work from Liu et al. Liu, Hu, Wei, Li and Jiang also considered the temperature and depth of discharge dependency in battery aging prediction and used the GPR model for battery SOH prediction. However, for second-life applications, the cost of disassembling retired batteries into cells is prohibitive Rallo, Benveniste, Gestoso and Amante. Since additional factors affect module degradation, such as electrical configuration, cell inhomogeneity, and cell-to-cell thermal interactions Tanim et al., it is essential to develop effective simulation tools for battery aging trajectory predictions at the module level to assess battery module level degradation. To account for these factors, researchers have attempted to integrate various physical models and simulate the aging performance of battery modules. Xia et al. Xia, Wang, Ren, Tao, Lu, Tian, Hu, Wang, Su, Chong, Jin and Lin (a), Xia, Yang, Wang, Ren, Sun, Feng and Qian (b) introduced a multi-physical model that combined electrochemical, thermal, fluid dynamics, and series-parallel circuit models. The authors also discussed the optimal method for balancing state-of-health (SOH) to prolong the lifespan of battery modules and packs. In a recent study Seger et al. a simple empirical model was proposed for second-life battery cells, to analyze how individual cell uncertainties could impact the module's capacity. Although a module-level model for SLBs was not established in Seger et al., it highlighted the need to consider the effects of cell uncertainties on the module level while developing aging models.

### 1.2. The economic model for second life battery

It is essential to demonstrate the profitability of using SLBs for specific applications by estimating their fair market value using a reliable method. Many previous studies have explored different cases of SLBs usage. For instance, Neubauer et al. Neubauer, Pesaran, Williams, Ferry and Eyer (b), Neubauer, Smith, Wood and Pesaran (a)

conducted early technoeconomic research on SLBs and evaluated the revenues obtained from various applications using the estimated battery price of 132\$  $kWh^{-1}$ . In Debnath, Ahmad and Habibi, Debnath et al. analyzed a different use of second life batteries as power backup for generation assets and demonstrated under certain conditions, the corresponding revenues would suppose a payback period of c.a. 1.5 years for the SLBs.

However, a recent study Börner et al. suggested that it was unnecessary to transfer SLBs into stationary storage systems related to the grid, since they might not be suitable for daily cycle demand, and the new battery price was low compared to the high repurposing cost. The results and conclusions presented in the literature vary significantly based on different applications, jurisdictions, and estimation models.

### 1.3. Article objective and structure

Based on previous research in the field, it is evident that scholars have approached the topic of retired Li-ion batteries from multiple perspectives, including aging models and economic analysis. However, despite the abundance of research, a comprehensive decision-making framework doesn't exist for retired Li-ion batteries. This paper proposes a decision-making model that integrates an aging prediction model and an economic evaluation model. The proposed model aims to provide researchers and industry professionals with a better understanding of SLBs' degradation and the various end-of-life strategies for retired Li-ion batteries. The novelty of this work is in three aspects: 1) our work first proposed a systematic model framework to evaluate retired Li-ion batteries for different second life applications; 2) the aging model we developed works for battery modules and packs, while most of the current aging prediction models are focused on cell-level; 3) the uncertainties in battery degradation is also well considered in our model, which would greatly affect the economic value of retired batteries and further impact the end-of-life decision.

This paper is structured as follows: Section 2 outlines the methodology used in this study. Section 3 provides a detailed explanation of our modeling approach for cell- and module-level prediction models, as well as the economic model. Section 4 presents the results of our prediction model at both the module and cell levels, along with the economic value calculated by our economic model. Finally, Section 5 concludes this work and suggests future research directions.

## 2. Methodology

### 2.1. Experimental dataset

The data used in this study was obtained from Vlijmen, Asinger, Lam, Cui, Ganapathi, Sun, Herring, Gopal, Geise, Deng, Thaman, Kang, Trewartha, Anapolsky, Storey, Gent, Braatz and Chueh. The dataset consisted of battery cycling data from 363 cylindrical Tesla cells, which utilized nickel-cobalt-aluminum (NCA) oxides as cathode materials and silicon oxides with graphite as anode materials. The aging experiment utilized 218 different combinations of cycling parameters. Each parameter was varied within certain ranges, as shown in Vlijmen et al. Figure S1. In this work, six cycling parameters (i.e. charge current in two stages, discharge current, charge cutoff voltage, discharge cutoff voltage, and constant voltage charge time), along with initial battery cell capacity and resistance values were selected as input features for model training. Additionally, the battery lifetime was evaluated, using capacity throughput-based equivalent full cycles (EFCs) Preger, Barkholtz, Fresquez, Campbell, Juba, Romàn-Kustas, Ferreira and Chalamala. Each cell underwent a sequence of diagnostic test and aging cycle test at a constant temperature (25°C). Typically, 100 aging cycles were conducted between each diagnostic cycle. Figure 1 shows the graphic demonstration of the test sequence. More details of these test protocols can be found in Vlijmen et al..

### 2.2. Decision-making model on end-of-life strategy

Figure 2 presents a comprehensive roadmap of the decision-making model for EOL strategies for retired Li-ion batteries. This model can be applicable to both OEMs and battery repurposing companies. The process starts with retired battery modules that are pre-disassembled from the original battery packs. The first step is to acquire the battery passport, which contains the battery basic information (including chemistry and usage profile). After conducting diagnostic tests, we can determine if the battery is qualified for reuse. The criteria of selecting qualified battery modules for reuse is not discussed in this paper. Here, we are only focused on the batteries pass the first testing phase. In the evaluation phase, the decision-making model is used to compare the values of the retired battery in all possible scenarios. With available first-life battery data from battery passport, the prediction model can first estimate the RUL of the retired battery in different second life use cases. The RUL can then be input into the economic model for further assessment. In the last phase, based on the comparison between estimated SLB values under different scenarios and recycling values, a decision can be made: reusing the batteries for second life application or direct recycling. If reusing

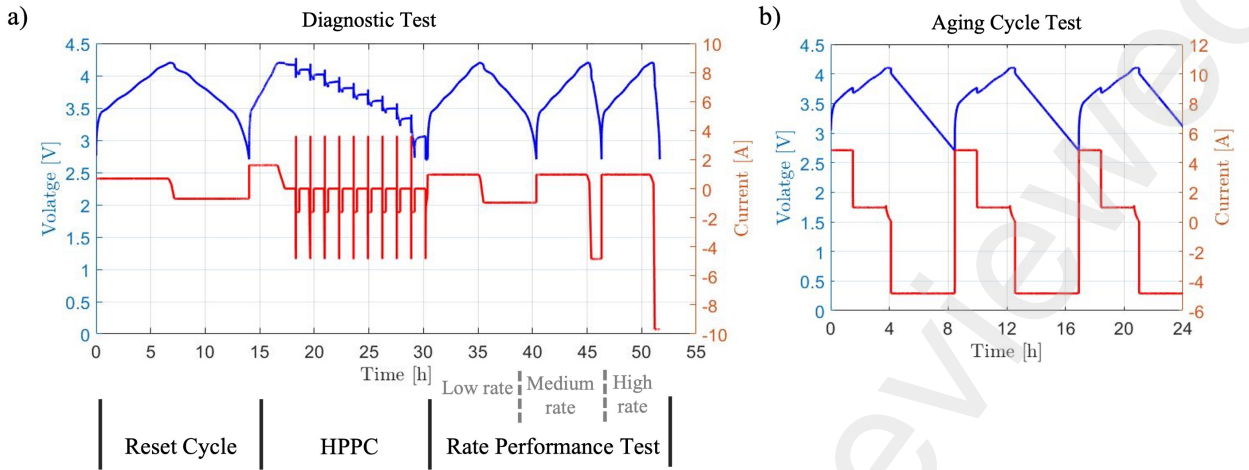


Figure 1: The aging test sequence of Tesla cells in experiment: a) diagnostic test, b) aging cycle test.

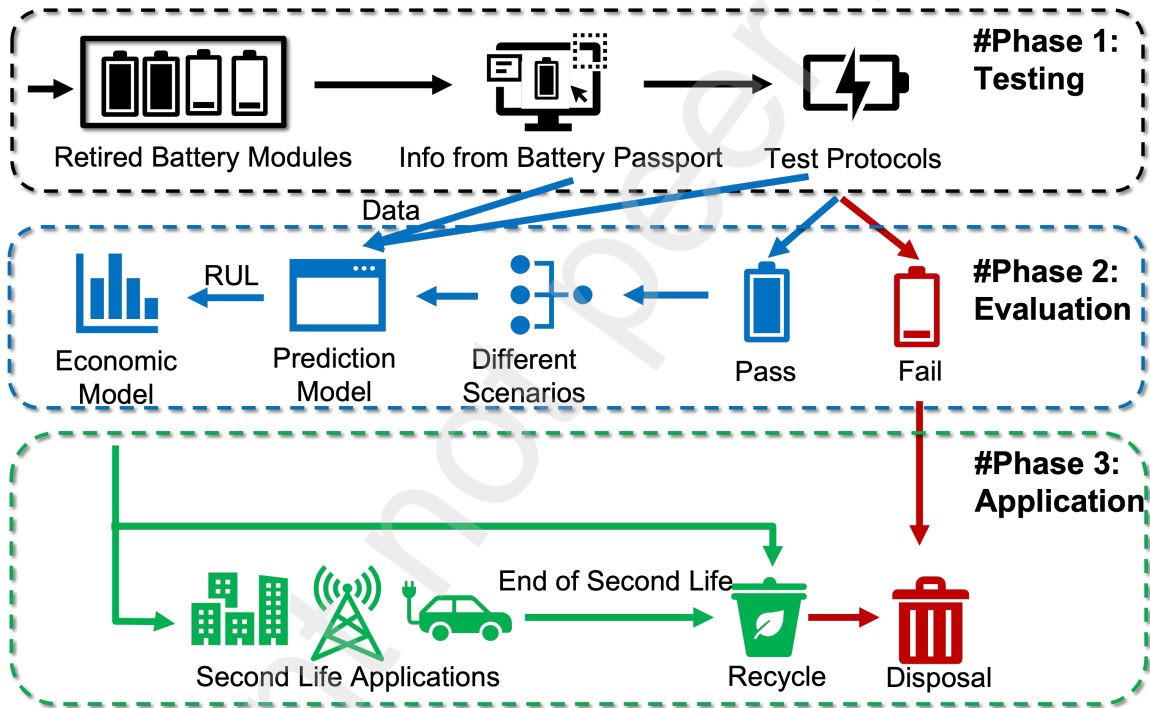


Figure 2: The roadmap of decision-making model for retired LIBs, including three critical steps: 1) testing phase, 2) evaluation phase, 3) application phase.

is preferred, the second life application with the highest value is output as the potential choice for the battery module. The decision-making model consists of two sub-models, the module-level prediction model and the economic model, which are introduced explicitly in the following section.

### 3. Sub-models of Decision-making Model

#### 3.1. Module-level Model Framework

The proposed module-level model comprises three main components: an equivalent circuit model (ECM), a GPR model, and a series-parallel circuit model. The module-level model predicts the aging trajectory of LIBs in their first and second life. Figure 3 provides an overview of the framework of the module-level model. For a given second life application, the power demand of the battery module is predefined. Using the module voltage measurements, the required battery module current can be calculated using module power divided by module voltage. The series-parallel circuit model is utilized to calculate the current flow across each cell of the battery module, depending on the module connections. A first-order ECM evaluates the voltage of every cell, using the corresponding cell current as an input. The outputs from the ECM and the cell current are then fed into the GPR model, which estimates the capacity degradation and resistance increase for all cells in the module. Subsequently, the series-parallel circuit model computes the module's capacity based on the capacity of each cell. During each simulation step, the parameters (capacity and resistance of each cell) in the ECM get updated for the next simulation step. Additionally, the voltage of the cell is utilized to calculate the module voltage and then update the input current to the battery module. As a result, the proposed model can simulate the battery module degradation.

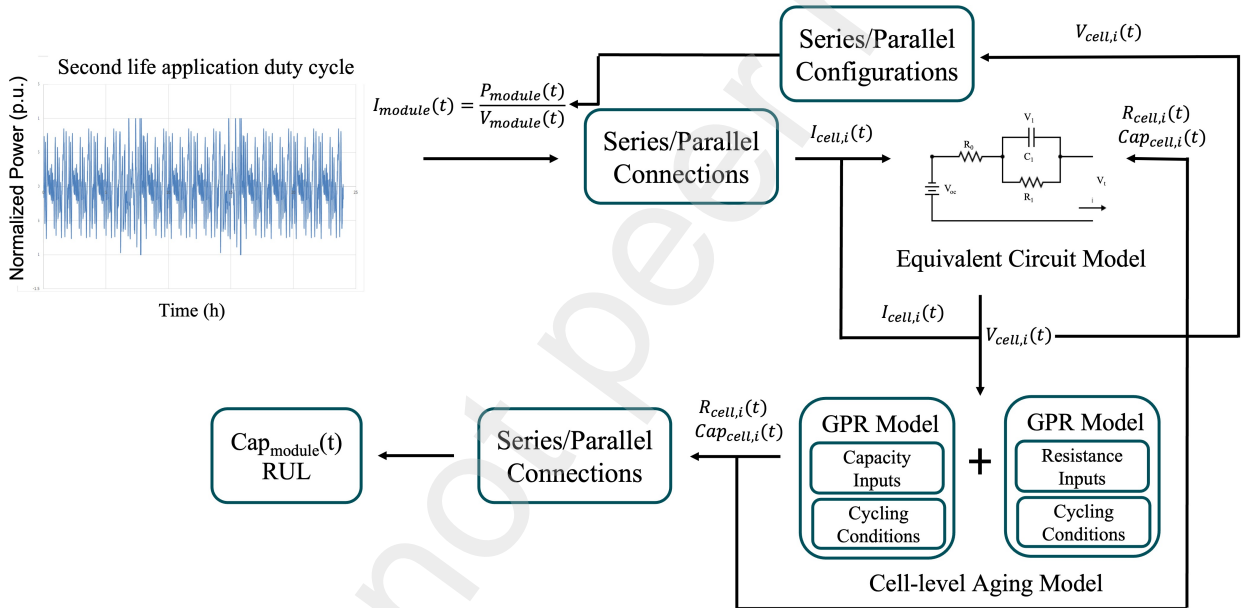


**Figure 3:** The framework of module-level degradation model, which consists of ECM, cell-level aging model and series-parallel circuit model.

#### 3.2. First Order Equivalent Circuit Model

ECM is commonly utilized in modeling the dynamic behavior of a battery, owing to its swift execution time, inherent simplicity, and relatively high accuracy Tran, Mathew, Janhunen, Panchal, Raahemifar, Fraser and Fowler (2021). In this study, the first-order ECM is chosen for its simplicity. The model structure is shown in Figure 3. More details of ECM can refer to Ahmed, Gazzarri, Onori, Habibi, Jackey, Rzemien, Tjong and LeSage. All the parameters in ECM can be identified by Hybrid Pulse Power Characterization (HPPC) test at different SOC values Nemes, Maria CIORNEI, Ruba and Martis.

#### 3.3. Gaussian Process Regression Model Structure

We develop our multi-step prediction model based on previous literature Liu et al., Takahashi, Allam and Onori (2023), as shown in Figure 4. The experimental data is used for model training. The input of the model is the combination of previous capacity data and the six cycling parameters, and the corresponding output is the capacity at time  $t + k$ . More specifically, the input and output vector are expressed in Equation 1 and Equation 2.

$$[Cap_{cell}(t - c), \dots, Cap_{cell}(t), C_{charge}, C_{discharge}, V_{charge}, V_{discharge}, t_{CVcharge}] \quad (1)$$

$$[Cap_{cell}(t + k), STD(t + k)] \quad (2)$$

In each recursion time step, e.g. at time  $t$ , the predicted capacity value is  $Cap_{cell}(t + 1)$ . This predicted value is also used to update the input vector for next step prediction, until it reaches to the time  $t + k$ . All further capacity values during the time  $t$  and time  $t + k$  can be obtained accordingly. In our work, we choose the Matern covariance function as the kernel function, as it was effective in different regression cases such as Richardson, Osborne and Howey. More modeling details can refer to this work Takahashi et al. (2023).

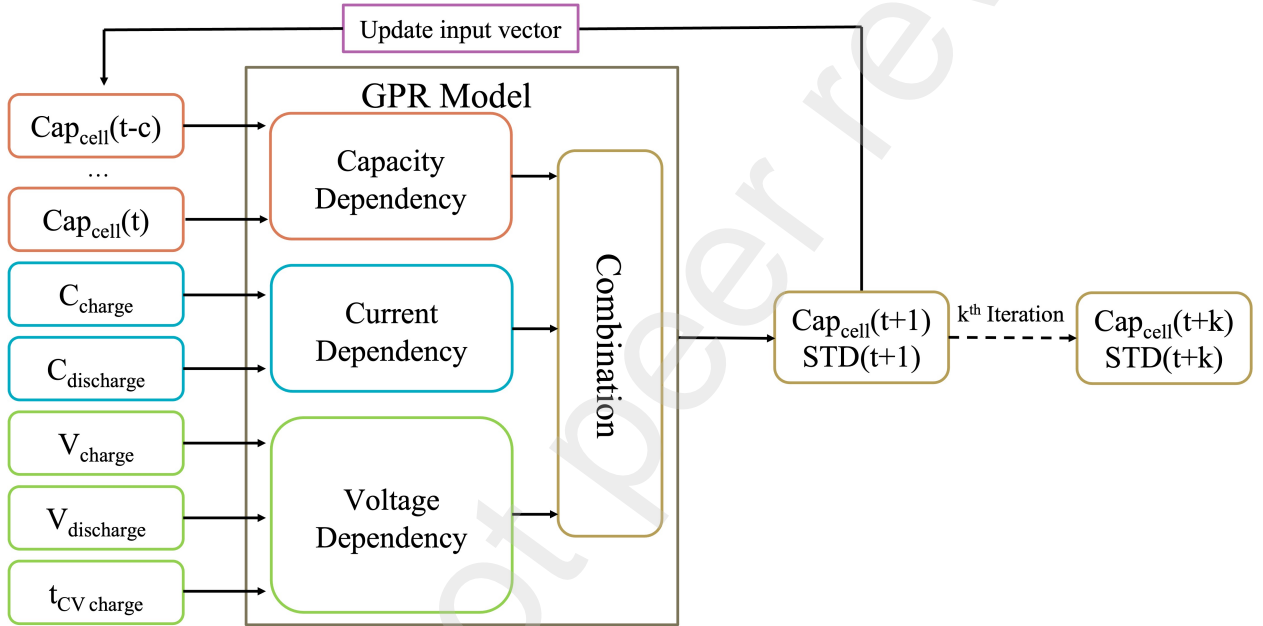


Figure 4: The structure of iterative cell-level GPR model for capacity prediction.

However, the GPR model usually requires a significant amount of computational time for training when facing a large dataset. To reduce the complexity of the GPR model, we implement a technique called bagging or bootstrapping. This involves creating  $m$  different bags of size  $n$  by randomly sampling from the whole dataset with replacement. More details about bagging can also refer to this work Takahashi et al. (2023).

In addition to the capacity degradation model, we apply the same method to develop a GPR model for resistance increase during cell degradation. In LIBs, among the most important resistance components in the battery are ohmic resistance and polarization resistance. The total resistance ( $R_{cell,i}$ ) of the cell is defined as the sum of these two resistances, and is used in the model. We build the resistance increase model based on the same GPR model structure by simply replacing the previous capacity data with  $R_{cell,i}$  data. The predicted resistance value is updated with ECM in every prediction step, along with the predicted capacity.

The models are evaluated on Root-Mean-Square Percent Error (RMSPE), Mean Absolute Percent Error (MAPE), and coefficient of determination ( $R^2$ ) with details in the Appendix.

### 3.4. Series-parallel Circuit Model

The series-parallel circuit model is established to calculate the current distribution and capacity of battery modules. This is necessary because the internal resistance and operating conditions vary from cell to cell due to the heterogeneity and cell connections of the battery module, resulting in effects of the different charging and discharging processes on

cells and modules Xia et al. (a). In a series connection, cells in the module operate under the same current, and the module voltage is the sum of all cells in series, as shown in Equation 3 and 4.

$$V_{module}(t) = \sum_{i=1}^u V_{cell,i}(t) \quad (3)$$

$$I_{module}(t) = I_{cell,1}(t) = I_{cell,2}(t) = \dots = I_{cell,u}(t) \quad (4)$$

On the other hand, in a parallel connection, cells operate at the same voltage as the module, and the module current is the sum of all currents into each cell, expressed in Equation 5 and 6.

$$V_{module}(t) = V_{cell,1}(t) = V_{cell,2}(t) = \dots = V_{cell,v}(t) \quad (5)$$

$$I_{module}(t) = \sum_{i=1}^v I_{cell,i}(t) \quad (6)$$

Similarly, the module capacity can be calculated by cell capacities using this model. When the module has a series connection, the module capacity is equal to the minimum capacity among all the cells in series (shown in Equation 7), whereas for parallel connection, the module capacity is the sum of all the cells in parallel (shown in Equation 8).

$$Cap_{module}(t) = \min(Cap_{cell,1}(t), Cap_{cell,2}(t), \dots, Cap_{cell,u}(t)) \quad (7)$$

$$Cap_{module}(t) = \sum_{i=1}^v Cap_{cell,i}(t) \quad (8)$$

### 3.5. Monte Carlo Simulation

In the context of battery module simulations, a single simulation cannot adequately capture the overall aging behavior due to uncertainties stemming from input variables and model prediction errors. To address this, Monte Carlo (MC) Simulation is introduced as a method to obtain statistics results of battery module degradation from multiple simulation results. Some researchers have combined MC simulation with battery aging models in the literature Zhang, Xiong, He and Pecht (2019), Tang, Zou, Yao, Lu, Xia and Gao (2019). In this study, the MC method is applied to account for heterogeneity of individual cells within the whole battery module and analyze battery module-level aging behavior through multiple simulations. Specifically, at the beginning, each cell in the module is randomly assigned a capacity and a resistance value from two normal distributions, where the values of  $\mu_c = 4.67$ ,  $\sigma_c = 0.005$ ,  $\mu_r = 0.026$ , and  $\sigma_r = 0.05$  are calculated from experimental data Vlijmen et al.. During each simulation iteration, at each time step, the mean and standard deviation of cells' capacity and resistance values are predicted via the GPR models. The actual  $Cap_{cell,i}(t)$  is then randomly chosen from the predicted capacity distribution, subject to a bounding condition that  $Cap_{cell,i}(t) \leq Cap_{cell,i}(t-1)$ . Similarly, the resistance of the cell is chosen from the predicted resistance distribution, subject to the opposite bounding condition that  $R_{cell,i}(t) \geq R_{cell,i}(t-1)$ . These bounding conditions are based on the assumption that as battery degrades, the capacity of the battery will decrease and the resistance will increase. After obtaining all the capacity values, Equation 7 and 8 are applied to calculate the overall capacity of the module in terms of series/parallel connections. The resistance and capacity values of each cell are also used to update the parameters in the ECM. This iterative process continued until the total capacity of the module reach the end-of-life condition, which is set at 60% of its initial capacity for second life. We select 100 as the number of iterations for MC, with details in SI Figure S5.

### 3.6. Economic Model

The economic model developed in this work is based on the present value of future cash flows to calculate the selling price of SLBs in different applications. Here, the selling price is the amount of money that buyers are willing to pay for the SLBs in the open market. The model includes two components: the Fair Market Value (FMV), which is the value a battery can provide regardless of its new or used condition, and the recycling value, which is calculated based on metal prices and recycling technologies.

The FMV of the used battery module after repurposing is calculated by setting the  $NPV_{new}$  and  $NPV_{used}$  to be the same. These two terms are calculated using Equation 9 and Equation 10, which take into account the predicted lifetimes of new and used batteries from degradation model.

$$NPV_{new} = \sum_{i=1}^{T_{new}} \frac{N \cdot e \cdot p_j \cdot \eta \cdot SOH_i \cdot DOD_j}{(1+r)^i} - e \cdot V_{e,new} - w \cdot V_{w,new} + \frac{P_r}{(1+r)^{T_{new}}} \quad (9)$$

$$NPV_{used} = \sum_{i=1}^{T_{used}} \frac{N \cdot e \cdot p_j \cdot \eta \cdot SOH_i \cdot DOD_j}{(1+r)^i} - e \cdot (V_{e,used} + C_r) + \frac{P_r}{(1+r)^{T_{used}}} \quad (10)$$

$$P_{selling,used} = e \cdot (V_{e,used} + C_r) \quad (11)$$

The  $NPV_{new}$  is determined by summing up the revenue generated by the new battery in a specific application over its lifetime, along with the depreciated recycling value, and then subtracting the cost of the energy and power components. Similarly, the  $NPV_{used}$  is calculated using the same method, but without considering in the cost of the power component. This is because the power component derived from EV batteries significantly surpasses the demands of stationary storage power components. If the  $NPV_{new} < 0$ , then the  $NPV_{used}$  is assumed to have a minimum value of 0. In Equation 10, no costs for the power component are included as we assume that the power component of used battery modules from electric cars is larger than the power requirements in a second life. Finally, the selling price of the SLBs can be estimated by Equation 11.

The decision on whether to recycle the SLBs or use them in an application is based on the highest selling price among the applications and the recycling price. If the selling price is less than the recycling price, the SLBs will be directly recycled. Otherwise, the SLBs will be recommended for use in the application with the highest selling price.

## 4. Results and Discussions

### 4.1. Cell-level GPR Prediction Results

Table 1 summarizes the prediction performances of the cell-level GPR model, including results with different numbers of capacity inputs using bagging technique. As shown in Figure 5, we can see that  $MAPE$ ,  $RMSE$  and standard deviation decrease, as well as the  $R^2$  increases with larger numbers of capacity inputs. This indicates the GPR model's performance improves with increased number of capacity input. However, when we compare the bagged GPR model performances of four and five capacity inputs, the difference is not significant. Therefore, we can conclude that it is unnecessary to further increase the number of capacity inputs. For bagging technique, it is always beneficial to have larger  $m$  and  $n$  values, as observed in SI Figure S1 and Figure S2. But excessively large  $m$  and  $n$  values can lead to long training times, counter to the goal of reducing computation time. Here, we choose  $m = 40$  and  $n = 50$ , as it shows a good model performance and no significant differences are observed among different bagging setups (shown in SI Table S1). Based on the foregoing analysis, we finally choose 5 previous capacities as one of the input parameters, and the bagging parameters are set to be the combination of  $m = 40$ ,  $n = 50$ . The results of train and test dataset for selected model setup is shown in SI Figure S9.

We also apply the bagging technique to train a second GPR model for resistance increase prediction, and the results are presented in Figure 6 and Table 2. As the number of resistance inputs increases, the model performances are improved, with decreased  $RMSE$ ,  $MAPE$ , standard deviation and increased  $R^2$ . We select five resistance inputs and the bagging setup of  $m = 40$ ,  $n = 50$  for the model training and subsequent simulation processes. The results of train and test dataset for selected model setup is shown in SI Figure S10.

No. of Input	2 Input	3 Input	4 Input	5 Input
<i>RMSPE</i> (%)	5.47	5.13	4.00	3.56
<i>MAPE</i> (%)	2.09	1.92	1.75	1.56
$R^2$	0.85	0.86	0.88	0.90
Standard deviation (mAh)	43.5	39.3	38.6	33.6

**Table 1**

Tabular summary of cell-level GPR model performances for capacity degradation.

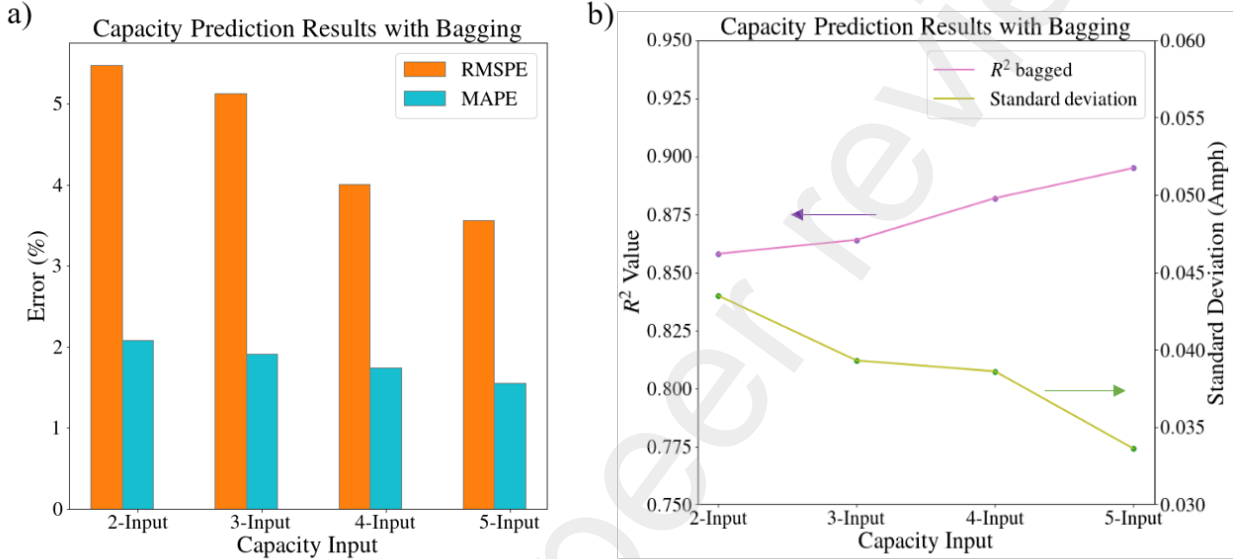


**Figure 5:** Graphic summary of cell-level GPR model performances for capacity degradation: a) *RMSPE* and *MAPE* results, b)  $R^2$  and standard deviation results.

No. of Input	2 Input	3 Input	4 Input	5 Input
<i>RMSPE</i> (%)	7.83	6.60	5.23	4.84
<i>MAPE</i> (%)	5.99	5.00	3.80	3.35
$R^2$	0.77	0.83	0.84	0.90
Standard deviation (mOhm)	1.84	1.63	1.52	1.44

**Table 2**

Tabular summary of cell-level GPR model performances for resistance increase

#### 4.2. Module-level Simulation Results

Considering the computational time of the model simulation and the most common commercial battery storage products in the market (listed in SI Table S3), the battery module capacity is set to be  $3.3kWh$  for simulation, which can be approximated as a 14P14S connection, meaning that 14 cells connect in parallel first and then connect in series. Table 3 is the summary of the approximated cycling profiles of battery modules from the actual demand profiles of three use cases in Comello and Reichelstein, Sbordone, Bertini, Di Pietra, Falvo, Genovese and Martirano (2015), Bauer, Nguyen, Jossen and Lygeros (2018). The approximation methods of each case are introduced explicitly in the Appendix.

We also simulate two real life scenarios for each use case. The first scenario involves LIBs received from the same first life application but retired at different SOH. The second scenario involve LIBs received from different first life applications with the same SOH. To simulate these scenarios, we assume the initial end-of-first-life points at 90%, 85%, and 80% SOH, and select three distinguished cell aging data from the experiment as different first life histories.

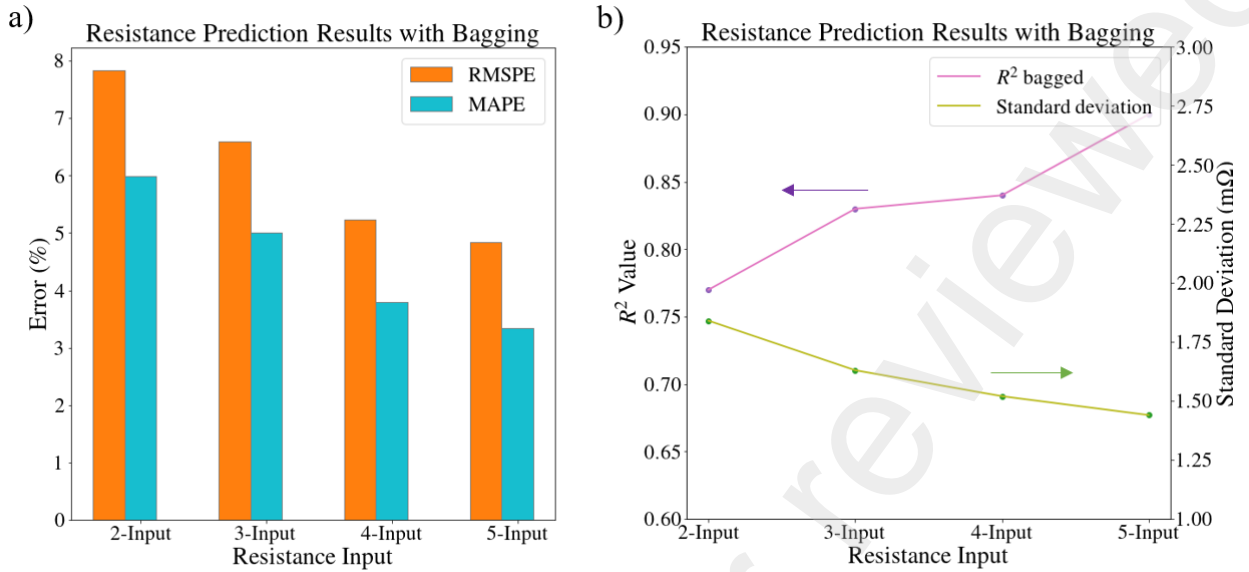


**Figure 6:** Graphic summary of cell-level GPR model performances for resistance increase: a) *RMSPE* and *MAPE* results, b)  $R^2$  and standard deviation results.

Use cases	Charge current	SOC range	operating	Constant voltage charge time	Discharge current
Residential application with photovoltaic(PV) system	C/5	10-90%		90 min	C/5
EV charging station	C/2	20-80%		90 min	C/2
Frequency regulation	C/5	30-50%		30 min	C/5

**Table 3**  
Cycling conditions of battery modules in different second life applications.

First life history (cell number in experiment)	Charge current	SOC range	operating	Constant voltage charge time	Discharge current
Case 1 (173)	C/2	0-90%		90 min	C/2
Case 2 (250)	C/5	0-90%		30 min	2C
Case 3 (148)	1C	0-90%		90 min	1C

**Table 4**  
Experimental cycling conditions of SLB modules in different first life histories.

In all simulation scenarios, we adopt experimental data as the initial input and subsequently simulate the degradation of battery modules in their second life.

#### 4.2.1. Effects of different second life duty profiles

Figure 7 presents the simulation results of three use cases with different duty profiles. Figures 7 (a-c) show the simulation results of a battery with the same first life history but different second life starting points and duty profiles. The initial capacity inputs for these three figures are selected from experimental data of cell number 173, whose cycling conditions are listed in Table 4, Case 1. In each figure, the starting points of the second life are kept the same for the

three second life duty profiles, which are 90%, 85%, and 80% SOH, respectively. From all three figures, it is evident that a battery module undergoing different second life duty profiles would have diverse aging patterns, especially in Figure 7 (a). In this figure, the battery module used in a frequency regulation application has the longest lifetime, approximately 800 EFCs in its second life, while in the residential application, the battery module lasts for only around 400 EFCs in its second life. However, the difference becomes less noticeable if the battery is used after reaching 80% SOH. As shown in Figure 7 (c), the lifetime difference between the two applications decreases to 100 EFCs, and the degradation curves become more similar. This indicates that the second life starting points also play a crucial role in battery second life, which is observed in SI Figure S8.

Limiting the SOC operating range can extend the lifetime of second life batteries, based on the simulation results of battery modules used in frequency regulation and residential applications. However, the effect of limiting the SOC operating range gradually diminishes as the battery ages. In contrast, the current has less impact on the battery aging in second life compared to the SOC operating range. This is demonstrated by the comparison of the case of EV charging station, which has a higher current but a smaller SOC operating range profile, and the case of residential application, which has a lower current but a larger SOC operating range profile, in Figure 7 (a). In summary, the effects of different second life duty profiles are noticeable and also related to the starting points of second life. Moreover, limiting the SOC operating range is found to be more beneficial than decreasing the current in second life applications.

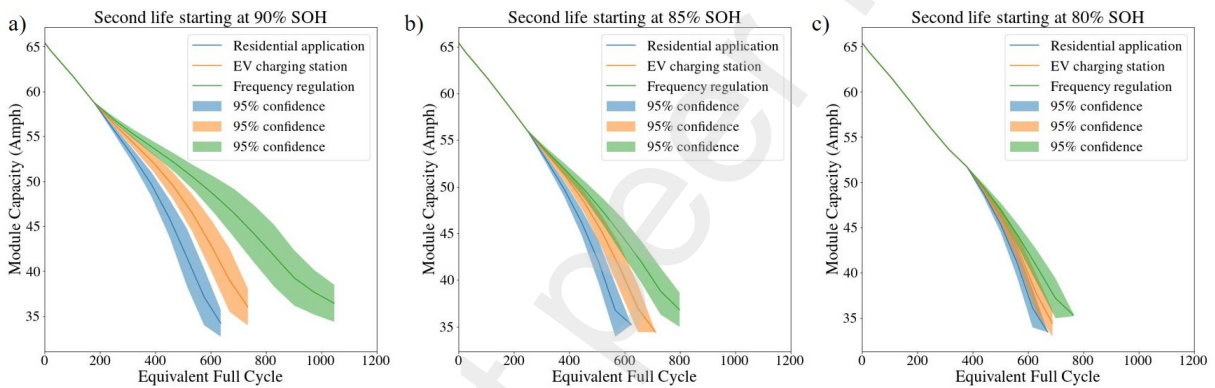


**Figure 7:** Simulation results showing distinguished battery module-level aging curves in different second life applications. Each subfigure corresponds to a different second life starting point: a) 90% SOH, b) 85% SOH, and c) 80% SOH. In each figure, different colors represent different second life applications.

#### 4.2.2. Effects of different first life histories

Three cell cycling data are selected as usage profiles for different first life applications, as shown in Table 4. Figure 8 (a-c) represents the SLB degradation behaviors of different first life histories and second life starting points. Batteries with different first life histories exhibit completely distinct aging behaviors in their second lives, regardless of when they are transferred from their original applications to second life applications. Upon closer examination of each figure, we also notice that batteries subjected to larger charge currents in their first life exhibit faster degradation in both their first and second lives, as indicated by the degradation curves of Case 1 and Case 2 in Figure 8 (a-c). However, discharge currents has a significantly lesser impact on battery degradation. In Case 2, the battery has a higher discharge current, but experiences less degradation compared to other two cases. These results suggest that optimizing the charge current can reduce battery degradation and extend battery lifetime for both first and second life.

In addition, when the second life starting point is at 90% SOH, the lifetime difference between Case 1 and Case 3 in second life is 289 EFCs, but it drops to 189 EFCs when the starting point is at 80% SOH. These results demonstrate that first life histories and second life starting points have a correlated effect on battery second life degradation. The lower the starting point, the less difference there is between the batteries from different first life histories. Similarly, a correlated effect is observed between different second life duty profiles and first life histories, as shown in SI Figure S6. The more intensive the second life duty profiles, the less discrepancy there is between different first life histories.

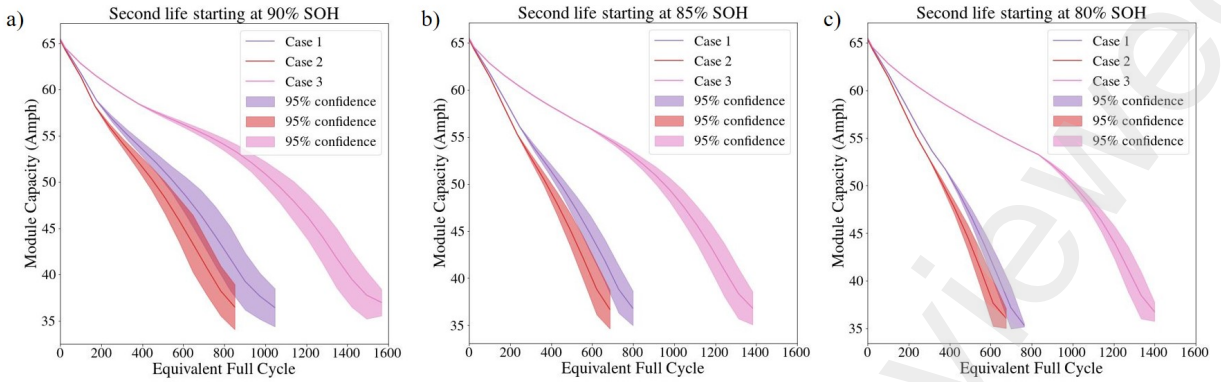


**Figure 8:** Simulation results of battery module-level degradation in frequency regulation application with different first life histories. Each subfigure corresponds to a different second life starting point: a) 90% SOH, b) 85% SOH, and c) 80% SOH. Different colors correspond to different first life histories.

### 4.3. Economic Model Simulation Result and Decision-making Process

Once the module-level prediction model has been established, an economic model that takes the predicted lifetime and SOH of the module capacity as inputs can be used to evaluate the selling price in different use cases. The values of model parameters are presented in SI Table S1. We simulate the selling prices of SLBs in three different second-life use cases with different second-life starting points (80% and 90% SOH) and first-life histories (Case 2 for high degradation and Case 3 for low degradation scenarios). Based on the price estimation in different scenarios, we can then make decisions by comparing the selling prices of SLBs with recycling prices. The results are summarized in Table 5. From Table 5, it is evident that the value of SLBs in residential applications is the lowest among the three second life applications. This is primarily due to the intensive cycling profile of residential use, which results in a shorter lifetime of the battery module, typically 1-3 years. Additionally, the unit revenue obtained from SLBs used in residential applications is also relatively small. Therefore, if a battery has already degraded to 80% SOH, it is not recommended to reuse it in a residential application. Instead, it would be better to either reuse it in other second life applications or recycle it. In comparison, SLBs used in EV charging stations and frequency regulation have higher selling prices. As shown in Table 5, for a retired battery module with a high degradation rate in its first life, the optimal strategy is to reuse it in an EV charging station for a second life. If the battery has a low degradation rate in its first life, it would be more beneficial to reuse it in a frequency regulation application. The highest selling price, i.e., \$ 273.4\$  $kWh^{-1}$ , is achieved when the SLBs are utilized in frequency regulation applications at 90% SOH with low capacity degradation in the first life. This phenomenon can be explained by the fact that SLBs used in frequency regulation applications have a longer lifetime, up to 6 years, but a lower unit revenue, whereas the unit revenue of SLBs used in EV charging stations is higher but the battery can only last for a maximum of 3 years. Therefore, the value of SLBs is mainly determined by their lifetime and unit revenue, but there is a trade-off between these two factors. For the three selected applications, in most cases, reusing is preferred over recycling. However, for residential applications, recycling is a better choice unless the received batteries have low degradation history and retired at 90% SOH. To summarize, the decision-making process is case-dependent, which aligns with our initial assumptions. Generally, the guideline for nickel-based LIBs is to leverage retired batteries in a second life application with higher unit revenue since the lifetime is limited, and a less demanding application will not improve it much. Unless the battery is well-utilized and monitored in its first life, i.e., degradation rate is controlled and minimized, and transferred into the second life at an early stage, the battery can be used for a light-duty application for a long time to maximize its residual value.

## 5. Conclusion and Future Work

In this work, a novel decision-making model designed for retired Li-ion batteries was proposed. The results demonstrate that the aging model is capable of predicting the lifetime range of retired Li-ion battery modules for various second life applications. The simulated battery module exhibits a lifetime of 1-6 years, depending on the use

Second life application	Second life starting SOH	First life degradation scenario	Battery selling price (\$ $kWh^{-1}$ )
Residential application	90%	High	45.2
		low	92.7
	80%	High	23.5
		low	28.3
EV charging station	90%	High	211.7
		low	227.9
	80%	High	109.7
		low	112.4
Frequency regulation	90%	High	159.3
		low	273.4
	80%	High	101.2
		low	114.5

**Table 5**

SLB selling prices under different scenarios. For each second life application, based on the battery first life degradation case and SOH, the price is estimated by the economic model.

case. Consequently, the selling prices of SLBs vary between 23.5-273.4 \$  $kWh^{-1}$  for different scenarios. Considering the degradation uncertainties, the end-of-life strategy is determined by comparing the selling prices with the recycling values under the best and worst scenarios. In general, reusing is preferred over recycling, particularly for leveraging SLBs in EV charging stations, due to their high unit revenue in most cases. However, for certain scenarios of residential applications, reusing is not profitable, and recycling appears to be a better option.

This work bridges the gap in the current research on second life batteries and provides a tool to decide whether to recycle or reuse the retired Li-ion battery modules from EVs. We believe this model can be useful for both OEMs, who want to know the selling values of their retired batteries, and recycling or repurposing companies, who try to find profitable applications to allocate SLBs.

The forthcoming studies will aim to enhance the completeness of the model by incorporating a reliable thermal model and incorporating additional experimental data from other chemical compositions, such as Lithium Iron Phosphate (LFP). Moreover, the scope of our model analysis can be extended to encompass more potential second-life applications, and actual user data from the energy storage market can be integrated to facilitate the emerging SLB industry. Furthermore, it is crucial to take into account the market size of possible second-life applications during the decision-making process. Once the market capacity for the most profitable application is met, the next best alternative should be considered.

## CRediT authorship contribution statement

**Jihan Zhuang:** Conceptualization of this study, Methodology, Software, Investigation, Writing - Original draft preparation. **Amadeus Bach:** Methodology - Economic model development, Writing - Review editing. **Bruis H. C. van Vlijmen:** Data curation, Experiment, Writing - Review editing.. **Stefan J. Reichelstein:** Supervision, Resources, Writing – review editing. **William Chueh:** Supervision, Resources, Writing – review editing. **Simona Onori:** Supervision, Resources, Writing – review editing. **Sally M. Benson:** Supervision, Resources, Writing – review editing.

## 6. Declaration of competing interest

The authors declare that they have no known competing financial interests or personal relationships that could have appeared to influence the work reported in this paper.

## 7. Acknowledgement

This research is supported by Stanford StorageX Initiative Circular Economy of Energy Storage (C2E2) consortium. The authors would also like to thank the researchers from the SLAC National Accelerator Laboratory for kindly sharing the battery data from their article Vlijmen et al..

Symbol	Unit	Explanation
$V_{discharge}$	V	The discharge cutoff voltage of cells in aging experiment
$V_{charge}$	V	The charge cutoff voltage of cells in aging experiment
$C_{discharge}$	C	The discharge C-rate of cells in aging experiment
$C_{charge}$	C	The charge C-rate of cells in aging experiment
$t_{CVcharge}$	minute	The constant voltage charge time of cells in aging experiment
$c$	Unitless	The number of input capacity values in GPR model
$k$	Unitless	The total number of iterative prediction steps in GPR model
$STD$	Ah	The standard deviation of cell capacity predicted by GPR model
$I_{cell,i}(t)$	A	The current of each individual cell in a module at time t
$V_{cell,i}(t)$	V	The voltage of each individual cell in a module at time t
$Cap_{cell,i}(t)$	Ah	The capacity of each individual cell in a module at time t
$R_{cell,i}(t)$	$\Omega$	The resistance of each individual cell in a module at time t
$I_{module}(t)$	A	The current of a battery module at time t
$V_{module}(t)$	V	The voltage of a battery module at time t
$Cap_{module}(t)$	Ah	The capacity of a battery module at time t
$P_{module}(t)$	kW	The power demand of a battery module at time t
$u$	Unitless	The number of cells connected in series in a battery module
$v$	Unitless	The number of cells connected in parallel in a battery module
$\mu_c$	Ah	The mean of cell capacities before aging experiment
$\sigma_c$	Ah	The standard deviation of cell capacities before aging experiment
$\mu_r$	$\Omega$	The mean of cell resistance before aging experiment
$\sigma_r$	$\Omega$	The standard deviation of cell resistance before aging experiment
$m$	Unitless	The number of GPR submodels in bagging technique
$n$	Unitless	The number of training samples in bagging technique
$NPV_{new}$	\$	The net profit value of a new battery module
$NPV_{used}$	\$	The net profit value of a used battery module
$V_{e,new}$	$\$ \cdot kWh^{-1}$	System price of energy component for a new battery
$V_{w,new}$	$\$ \cdot kW^{-1}$	System price of power component for a new battery
$V_{e,used}$	$\$ \cdot kWh^{-1}$	System price all components for a used battery
$w$	kW	Power of new battery
$e$	kWh	Energy storage capacity of a new battery
$p_j$	\$	The unit revenue of different second life applications per kWh stored
$\eta$	Unitless	Round-trip efficiency factor of the storage system
$SOH_i$	Unitless	Battery capacity state of health
$DOD_j$	Unitless	Battery state of charge operating range in different applications
$N$	Unitless	Number of charge and discharge cycles per year
$r$	Unitless	Discount rate
$C_r$	$\$ \cdot kWh^{-1}$	Repurposing cost of used battery
$P_r$	$\$ \cdot kWh^{-1}$	Recycling price of battery
$T_{new}$	year	Lifetime of the new battery from original SOH to 60% SOH
$T_{used}$	year	Lifetime of the used battery from original SOH to 60% SOH

**Table 6**  
Nomenclature

## 8. Glossary

## A. Appendix

### A.1. GPR Model evaluation metrics

In order to evaluate the GPR model performance, three performance metrics are chosen to compare with different model settings. These indicators are calculated through both first life and second life of batteries, representing the model performance over whole aging trajectories. Root-Mean-Square Percent Error (RMSPE) is one of the most popular indicators to reflect the deviation between the predicted values and real values.

$$\sqrt{\frac{1}{N} \cdot \sum_{i=1}^N \left( \frac{y_{i,pred}}{y_{i,exp}} - 1 \right)^2} \cdot 100\% \quad (12)$$

where  $y_{i,pred}$  and  $y_{i,exp}$  are the predicted value and experimental value in training or testing dataset respectively. Another indicator is Mean Absolute Percent Error (MAPE), which reflects the actual deviation of the predicted values. It is shown in Equation 13:

$$\frac{1}{N} \sum_{i=1}^N \left| \frac{y_{i,pred}}{y_{i,exp}} - 1 \right| \cdot 100\% \quad (13)$$

The last indicator is also very commonly used, which is called the coefficient of determination ( $R^2$ ). It is a measure that provides information about the goodness of fit of a model. The Equation 14 is used to calculate  $R^2$ :

$$1 - \frac{SSR}{SST} = 1 - \frac{\sum_{i=1}^N (y_{i,pred} - y_{i,exp})^2}{\sum_{i=1}^N (y_{i,pred} - y_{mean})^2} \quad (14)$$

where SSR stands for the sum squared regression and SST represents the total sum of squares of the given model. The smaller the RMSPE and MPE, the more accurate the predicted results. However,  $R^2$  is between zero and one, and the closer to one, the better the predicted results.

### A.2. Second life application profile approximation details

#### A.2.1. Residential application combined with PV system

In Comello and Reichelstein, a typical daily pattern of household power demand is presented. The demand profile illustrates that the battery is charged during the daytime when the PV system is functioning and discharged at night. To simplify the analysis, we can assume that the battery undergoes one constant charge and discharge cycle per day. From the demand profile example provided in Comello and Reichelstein Figure 2, we can also assume that the battery charges and discharges completely roughly around 5 hours, which equals the minimum C-rate observed in the experiment (C/5). The usage of battery is also 1 duty cycle per day based on this demand profile.

#### A.2.2. EV charging station application

Several previous studies have investigated the use of stationary lithium-ion batteries (SLBs) to provide peak shaving services for electric vehicle (EV) charging stations Sbordone et al. (2015); Deng, Zhang, Luo and Mu (2021); Kamath, Arsenault, Kim and Ancil. Typically, the battery provides power when the demand for EV charging exceeds the power limit designated for the grid. In Sbordone et al. (2015), sampled test results of battery usage during the charging process were provided. The demand profile for EV charging stations was shown to be dynamic and case-dependent. By adjusting the power threshold, a control strategy proposed in Sbordone et al. (2015) can assume that the battery would mostly operate in a designed pattern. Additionally, the SLB storage system is constrained not to exceed 80% of its maximum power for protection purposes. Based on these two assumptions, Test Profile 2 in Sbordone et al. (2015) can serve as a demonstration for our model simulation. The current withdrawn from the battery module is roughly equal to C/2, and the state of charge (SOC) range is kept between 20% and 80%, which are common in EV charging station applications Yang and Ribberink. The battery usage is also set to be 1 duty cycle per day. In real-world applications, specific numerical values may be updated to suit a given use case.

### A.2.3. Frequency Regulation for Grid Application

In power systems, the frequency of the grid is affected by deviations between supply and demand Bauer et al. (2018). An excess of generation results in an increase in frequency, while an excess of demand leads to a decrease in frequency. The purpose of providing a frequency regulation service is to maintain balance between grid demand and supply by compensating for deviations from the nominal frequency. To simulate the battery demand profile for our model, we use the battery demand profile from Bauer et al. (2018). However, we must make several assumptions to approximate this demand profile for use as the input for our model. According to the analysis in Bauer et al. (2018), most of the currents extracted from a BESS fall within the range of  $-10A$  to  $10A$  for a battery pack with a capacity of  $300Ah$ . This range is much smaller than the minimum C-rate ( $C/5$ ) observed in our experiment; therefore, we select  $C/5$  as the charge and discharge C-rate for our simulation. Additionally, since the battery maintains its SOC within a relatively narrow range, we choose the corresponding experimental voltages based on the upper and lower SOC boundaries, which are 50% and 30% SOC, respectively, as reported in Bauer et al. (2018) Table 3. The usage of battery according to Bauer et al. (2018) Table 1 is 5.73 EFCS per week, which is about 4 duty cycle per day.

## References

- , a. Monthly energy review - september 2022. U.S Energy Information Administration , 282.
- , b. Toyota to collaborate with redwood materials on a sustainable, closed-loop electrified vehicle battery ecosystem. Toyota Newsroom URL: <https://pressroom.toyota.com/toyota-to-collaborate-with-redwood-materials-on-a-sustainable-closed-loop-electrified-vehicle-battery-ecosystem/>
- Ahmed, R., Gazzari, J., Onori, S., Habibi, S., Jackey, R., Rzemien, K., Tjong, J., LeSage, J., . Model-based parameter identification of healthy and aged li-ion batteries for electric vehicle applications 4, 233–247. URL: <https://www.sae.org/content/2015-01-0252/>, doi:10.4271/2015-01-0252.
- Arunachalam, H., Onori, S., 2019. Full homogenized macroscale model and pseudo-2-dimensional model for lithium-ion battery dynamics: Comparative analysis, experimental verification and sensitivity analysis. Journal of The Electrochemical Society 166, A1380. URL: <https://dx.doi.org/10.1149/2.0051908jes>, doi:10.1149/2.0051908jes.
- Attia, P.M., Grover, A., Jin, N., Severson, K.A., Markov, T.M., Liao, Y.H., Chen, M.H., Cheong, B., Perkins, N., Yang, Z., Herring, P.K., Aykol, M., Harris, S.J., Braatz, R.D., Ermon, S., Chueh, W.C., . Closed-loop optimization of fast-charging protocols for batteries with machine learning. Nature 578, 397–402. URL: <http://www.nature.com/articles/s41586-020-1994-5>, doi:10.1038/s41586-020-1994-5.
- Bauer, M., Nguyen, T.T., Jossen, A., Lygeros, J., 2018. Evaluating frequency regulation operated on two stationary energy systems with batteries from electric vehicles. Energy Procedia 155, 32–43. URL: <https://www.sciencedirect.com/science/article/pii/S1876610218310233>, doi:<https://doi.org/10.1016/j.egypro.2018.11.068>. 12th International Renewable Energy Storage Conference, IRES 2018, 13-15 March 2018, Düsseldorf, Germany.
- Baumann, M., Rohr, S., Lienkamp, M., . Cloud-connected battery management for decision making on second-life of electric vehicle batteries, in: 2018 Thirteenth International Conference on Ecological Vehicles and Renewable Energies (EVER), IEEE, pp. 1–6. URL: <https://ieeexplore.ieee.org/document/8362355/>, doi:10.1109/EVER.2018.8362355.
- Börner, M.F., Frieges, M.H., Späth, B., Spütz, K., Heimes, H.H., Sauer, D.U., Li, W., . Challenges of second-life concepts for retired electric vehicle batteries. Cell Reports Physical Science , 101095URL: <https://linkinghub.elsevier.com/retrieve/pii/S2666386422003976>, doi:10.1016/j.xcrp.2022.101095.
- Chen, M., Ma, X., Chen, B., Arsenault, R., Karlson, P., Simon, N., Wang, Y., 2019. Recycling end-of-life electric vehicle lithium-ion batteries. Joule 3, 2622–2646. URL: <https://www.sciencedirect.com/science/article/pii/S254243511930474X>, doi:<https://doi.org/10.1016/j.joule.2019.09.014>.
- Chu, A., Allam, A., Cordoba Arenas, A., Rizzoni, G., Onori, S., 2020. Stochastic capacity loss and remaining useful life models for lithium-ion batteries in plug-in hybrid electric vehicles. Journal of Power Sources 478, 228991. URL: <https://www.sciencedirect.com/science/article/pii/S037877532031288X>, doi:<https://doi.org/10.1016/j.jpowsour.2020.228991>.
- Comello, S., Reichelstein, S., . The emergence of cost effective battery storage. Nature Communications 10, 2038. URL: <http://www.nature.com/articles/s41467-019-09988-z>, doi:10.1038/s41467-019-09988-z.
- Debnath, U.K., Ahmad, I., Habibi, D., . Gridable vehicles and second life batteries for generation side asset management in the smart grid. International Journal of Electrical Power & Energy Systems 82, 114–123. URL: <https://linkinghub.elsevier.com/retrieve/pii/S0142061516303635>, doi:10.1016/j.ijepes.2016.03.006.
- Deng, Y., Zhang, Y., Luo, F., Mu, Y., 2021. Operational planning of centralized charging stations utilizing second-life battery energy storage systems. IEEE Transactions on Sustainable Energy 12, 387–399. doi:10.1109/TSTE.2020.3001015.
- Duarte, E., . Mercedes strikes second-life EV battery pact with canadian startup moment energy. Bloomberg URL: <https://www.bloomberg.com/news/articles/2022-07-06/mercedes-strikes-second-life-battery-pact-with-canadian-startup?leadSource=uverify%20wall>.
- Hu, X., Che, Y., Lin, X., Onori, S., 2021. Battery health prediction using fusion-based feature selection and machine learning. IEEE Transactions on Transportation Electrification 7, 382–398. doi:10.1109/TTE.2020.3017090.
- JEAN KUMAGAI, . LITHIUM-ION BATTERY RECYCLING FINALLY TAKES OFF IN NORTH AMERICA AND EUROPE URL: <https://spectrum.ieee.org/lithiumion-battery-recycling-finally-takes-off-in-north-america-and-europe>.
- Johnen, M., Pitzen, S., Kamps, U., Kateri, M., Dechent, P., Sauer, D.U., . Modeling long-term capacity degradation of lithium-ion batteries. Journal of Energy Storage 34, 102011. URL: <https://linkinghub.elsevier.com/retrieve/pii/S2352152X20318466>, doi:10.1016/j.est.2020.102011.

- Jones, P.K., Stimming, U., Lee, A.A., . Impedance-based forecasting of lithium-ion battery performance amid uneven usage 13, 4806. URL: <https://www.nature.com/articles/s41467-022-32422-w>, doi:10.1038/s41467-022-32422-w.
- Justin Westbrook, . How the tesla model s and model x batteries degrade over 200,000 miles URL: <https://www.motortrend.com/news/tesla-model-s-x-battery-health-over-time/#:~:text=Tesla%20claims%20that%20up%20to,Model%20S%20and%20X%20vehicles>.
- Kamath, D., Arsenault, R., Kim, H.C., Anctil, A., . Economic and environmental feasibility of second-life lithium-ion batteries as fast-charging energy storage 54, 6878–6887. URL: <https://doi.org/10.1021/acs.est.9b05883>, doi:10.1021/acs.est.9b05883. publisher: American Chemical Society.
- Kebir, N., Leonard, A., Downey, M., Jones, B., Rabie, K., Bhagavathy, S.M., Hirmer, S.A., . Second-life battery systems for affordable energy access in kenyan primary schools 13, 1374. URL: <https://doi.org/10.1038/s41598-023-28377-7>, doi:10.1038/s41598-023-28377-7.
- Li-Cycle, . Lithium-ion battery recycling. URL: <https://li-cycle.com>.
- Liu, K., Hu, X., Wei, Z., Li, Y., Jiang, Y., . Modified gaussian process regression models for cyclic capacity prediction of lithium-ion batteries. *IEEE Transactions on Transportation Electrification* 5, 1225–1236. URL: <https://ieeexplore.ieee.org/document/8853281/>, doi:10.1109/TTE.2019.2944802.
- Lucu, M., Martinez-Laserna, E., Gandiaga, I., Camblong, H., . A critical review on self-adaptive li-ion battery ageing models. *Journal of Power Sources* 401, 85–101. URL: <https://linkinghub.elsevier.com/retrieve/pii/S0378775318309297>, doi:10.1016/j.jpowsour.2018.08.064.
- Mathews, I., Xu, B., He, W., Barreto, V., Buonassisi, T., Peters, I.M., . Technoeconomic model of second-life batteries for utility-scale solar considering calendar and cycle aging. *Applied Energy* 269, 115127. URL: <https://linkinghub.elsevier.com/retrieve/pii/S0306261920306395>, doi:10.1016/j.apenergy.2020.115127.
- Nemes, R.O., Maria CIORNEI, S., Ruba, M., Martis, C., . Parameters identification using experimental measurements for equivalent circuit lithium-ion cell models, in: 2019 11th International Symposium on Advanced Topics in Electrical Engineering (ATEE), IEEE. pp. 1–6. URL: <https://ieeexplore.ieee.org/document/8724878/>, doi:10.1109/ATEE.2019.8724878.
- Neubauer, J., Smith, K., Wood, E., Pesaran, A., a. Identifying and overcoming critical barriers to widespread second use of PEV batteries. URL: <http://www.osti.gov/servlets/purl/1171780/>, doi:10.2172/1171780.
- Neubauer, J.S., Pesaran, A., Williams, B., Ferry, M., Eyer, J., b. A techno-economic analysis of PEV battery second use: Repurposed-battery selling price and commercial and industrial end-user value, pp. 2012–01–0349. URL: <https://www.sae.org/content/2012-01-0349/>, doi:10.4271/2012-01-0349.
- Ng, M.F., Zhao, J., Yan, Q., Conduit, G.J., Seh, Z.W., . Predicting the state of charge and health of batteries using data-driven machine learning. *Nature Machine Intelligence* 2, 161–170. URL: <http://www.nature.com/articles/s42256-020-0156-7>, doi:10.1038/s42256-020-0156-7.
- Petit, M., Prada, E., Sauvart-Moynot, V., 2016. Development of an empirical aging model for li-ion batteries and application to assess the impact of vehicle-to-grid strategies on battery lifetime. *Applied Energy* 172, 398–407. URL: <https://www.sciencedirect.com/science/article/pii/S0306261916304500>, doi:https://doi.org/10.1016/j.apenergy.2016.03.119.
- Pinson, M.B., Bazant, M.Z., . Theory of SEI formation in rechargeable batteries: Capacity fade, accelerated aging and lifetime prediction 160, A243–A250. URL: <https://iopscience.iop.org/article/10.1149/2.044302jes>, doi:10.1149/2.044302jes.
- Prada, E., Di Domenico, D., Creff, Y., Bernard, J., Sauvart-Moynot, V., Huet, F., . Simplified electrochemical and thermal model of LiFePO<sub>4</sub>-graphite li-ion batteries for fast charge applications 159, A1508–A1519. URL: <https://iopscience.iop.org/article/10.1149/2.064209jes>, doi:10.1149/2.064209jes.
- Preger, Y., Barkholtz, H.M., Fresquez, A., Campbell, D.L., Juba, B.W., Romàn-Kustas, J., Ferreira, S.R., Chalamala, B., . Degradation of commercial lithium-ion cells as a function of chemistry and cycling conditions 167, 120532. URL: <https://iopscience.iop.org/article/10.1149/1945-7111/abae37>, doi:10.1149/1945-7111/abae37.
- Rallo, H., Benveniste, G., Gestoso, I., Amante, B., . Economic analysis of the disassembling activities to the reuse of electric vehicles li-ion batteries. *Resources, Conservation and Recycling* 159, 104785. URL: <https://linkinghub.elsevier.com/retrieve/pii/S0921344920301063>, doi:10.1016/j.resconrec.2020.104785.
- Rechkemmer, S.K., Zang, X., Zhang, W., Sawodny, O., 2019. Empirical li-ion aging model derived from single particle model. *Journal of Energy Storage* 21, 773–786. URL: <https://www.sciencedirect.com/science/article/pii/S2352152X18307588>, doi:https://doi.org/10.1016/j.est.2019.01.005.
- Richardson, R.R., Osborne, M.A., Howey, D.A., . Gaussian process regression for forecasting battery state of health. *Journal of Power Sources* 357, 209–219. URL: <https://linkinghub.elsevier.com/retrieve/pii/S0378775317306250>, doi:10.1016/j.jpowsour.2017.05.004.
- Richardson, R.R., Osborne, M.A., Howey, D.A., 2017. Gaussian process regression for forecasting battery state of health. *Journal of Power Sources* 357, 209–219. URL: <https://www.sciencedirect.com/science/article/pii/S0378775317306250>, doi:https://doi.org/10.1016/j.jpowsour.2017.05.004.
- Sbordone, D., Bertini, I., Di Pietra, B., Falvo, M., Genovese, A., Martirano, L., 2015. Ev fast charging stations and energy storage technologies: A real implementation in the smart micro grid paradigm. *Electric Power Systems Research* 120, 96–108. URL: <https://www.sciencedirect.com/science/article/pii/S0378779614002880>, doi:https://doi.org/10.1016/j.epsr.2014.07.033. smart Grids: World's Actual Implementations.
- Segeer, P.V., Thivel, P.X., Riu, D., . A second life li-ion battery ageing model with uncertainties: From cell to pack analysis. *Journal of Power Sources* 541, 231663. URL: <https://linkinghub.elsevier.com/retrieve/pii/S0378775322006619>, doi:10.1016/j.jpowsour.2022.231663.
- Severson, K.A., Attia, P.M., Jin, N., Perkins, N., Jiang, B., Yang, Z., Chen, M.H., Aykol, M., Herring, P.K., Fraggedakis, D., Bazant, M.Z., Harris, S.J., Chueh, W.C., Braatz, R.D., . Data-driven prediction of battery cycle life before capacity degradation 4, 383–391. URL:

- <https://www.nature.com/articles/s41560-019-0356-8>, doi:10.1038/s41560-019-0356-8.
- Sun, S.I., Chipperfield, A.J., Kiaee, M., Wills, R.G., 2018. Effects of market dynamics on the time-evolving price of second-life electric vehicle batteries. *Journal of Energy Storage* 19, 41–51. URL: <https://www.sciencedirect.com/science/article/pii/S2352152X17306084>, doi:<https://doi.org/10.1016/j.est.2018.06.012>.
- Takahashi, A., Allam, A., Onori, S., 2023. Evaluating the feasibility of batteries for second-life applications using machine learning. *iScience* 26, 106547. URL: <https://www.sciencedirect.com/science/article/pii/S2589004223006247>, doi:<https://doi.org/10.1016/j.isci.2023.106547>.
- Tang, X., Zou, C., Yao, K., Lu, J., Xia, Y., Gao, F., 2019. Aging trajectory prediction for lithium-ion batteries via model migration and bayesian monte carlo method. *Applied Energy* 254, 113591. URL: <https://www.sciencedirect.com/science/article/pii/S0306261919312656>, doi:<https://doi.org/10.1016/j.apenergy.2019.113591>.
- Tanim, T.R., Shirk, M.G., Bewley, R.L., Dufek, E.J., Liaw, B.Y., . Fast charge implications: Pack and cell analysis and comparison. *Journal of Power Sources* 381, 56–65. URL: <https://linkinghub.elsevier.com/retrieve/pii/S0378775318301009>, doi:10.1016/j.jpowsour.2018.01.091.
- Tran, M.K., Mathew, M., Janhunen, S., Panchal, S., Raahemifar, K., Fraser, R., Fowler, M., 2021. A comprehensive equivalent circuit model for lithium-ion batteries, incorporating the effects of state of health, state of charge, and temperature on model parameters. *Journal of Energy Storage* 43, 103252. URL: <https://www.sciencedirect.com/science/article/pii/S2352152X2100949X>, doi:<https://doi.org/10.1016/j.est.2021.103252>.
- Vlijmen, B.V., Asinger, P.A., Lam, V., Cui, X., Ganapathi, D., Sun, S., Herring, P.K., Gopal, C.B., Geise, N., Deng, H.D., Thaman, H.L., Kang, S.D., Trewartha, A., Anapolsky, A., Storey, B.D., Gent, W.E., Braatz, R.D., Chueh, W.C., . Interpretable data-driven modeling reveals complexity of battery aging. URL: <https://chemrxiv.org/engage/chemrxiv/article-details/644b044280f4b75b533b1c9d>, doi:10.26434/chemrxiv-2023-zdl2n.
- Weaver, T., Allam, A., Onori, S., 2020. A novel lithium-ion battery pack modeling framework - series-connected case study, in: 2020 American Control Conference (ACC), pp. 365–372. doi:10.23919/ACC45564.2020.9147546.
- Xia, Q., Wang, Z., Ren, Y., Tao, L., Lu, C., Tian, J., Hu, D., Wang, Y., Su, Y., Chong, J., Jin, H., Lin, Y., a. A modified reliability model for lithium-ion battery packs based on the stochastic capacity degradation and dynamic response impedance. *Journal of Power Sources* 423, 40–51. URL: <https://linkinghub.elsevier.com/retrieve/pii/S0378775319302812>, doi:10.1016/j.jpowsour.2019.03.042.
- Xia, Q., Yang, D., Wang, Z., Ren, Y., Sun, B., Feng, Q., Qian, C., b. Multiphysical modeling for life analysis of lithium-ion battery pack in electric vehicles. *Renewable and Sustainable Energy Reviews* 131, 109993. URL: <https://linkinghub.elsevier.com/retrieve/pii/S1364032120302847>, doi:10.1016/j.rser.2020.109993.
- Xiong, R., Li, L., Tian, J., . Towards a smarter battery management system: A critical review on battery state of health monitoring methods. *Journal of Power Sources* 405, 18–29. URL: <https://linkinghub.elsevier.com/retrieve/pii/S037877531831111X>, doi:10.1016/j.jpowsour.2018.10.019.
- Yang, D., Zhang, X., Pan, R., Wang, Y., Chen, Z., . A novel gaussian process regression model for state-of-health estimation of lithium-ion battery using charging curve. *Journal of Power Sources* 384, 387–395. URL: <https://linkinghub.elsevier.com/retrieve/pii/S0378775318302398>, doi:10.1016/j.jpowsour.2018.03.015.
- Yang, L., Ribberink, H., . Investigation of the potential to improve DC fast charging station economics by integrating photovoltaic power generation and/or local battery energy storage system 167, 246–259. URL: <https://linkinghub.elsevier.com/retrieve/pii/S0360544218321431>, doi:10.1016/j.energy.2018.10.147.
- Zhang, Y., Xiong, R., He, H., Pecht, M.G., 2019. Lithium-ion battery remaining useful life prediction with box–cox transformation and monte carlo simulation. *IEEE Transactions on Industrial Electronics* 66, 1585–1597. doi:10.1109/TIE.2018.2808918.
- Zhu, J., Mathews, I., Ren, D., Li, W., Cogswell, D., Xing, B., Sedlatschek, T., Kantareddy, S.N.R., Yi, M., Gao, T., Xia, Y., Zhou, Q., Wierzbicki, T., Bazant, M.Z., 2021. End-of-life or second-life options for retired electric vehicle batteries. *Cell Reports Physical Science* 2, 100537. URL: <https://www.sciencedirect.com/science/article/pii/S2666386421002484>, doi:<https://doi.org/10.1016/j.xcrp.2021.100537>.